Journal of Nuclear Materials 382 (2008) 223–228

Contents lists available at ScienceDirect

Journal of Nuclear Materials

journal homepage: www.elsevier.com/locate/jnucmat

Formation of austenite in high Cr ferritic/martensitic steels by high fluence neutron irradiation

Z. Lu *, R.G. Faulkner, T.S. Morgan

IPTME, Loughborough University, Loughborough LE11 3U, UK

ARTICLE INFO

PACS:
81.30.−t
61.80.−x

ABSTRACT

High Cr ferritic/martensitic steels are leading candidates for structural components of future fusion reactors and new generation fission reactors due to their excellent swelling resistance and thermal properties. A commercial grade 12%CrMoVNb ferritic/martensitic stainless steel in the form of parent plate and off-normal weld materials was fast neutron irradiated up to 33 dpa (1.1×10^{-6} dpa/s) at 400 °C and 28 dpa (1.7×10^{-6} dpa/s) at 465 °C, respectively. TEM investigation shows that the fully martensitic weld metal transformed to a duplex austenite/ferrite structure due to high fluence neutron irradiation, the austenite was heavily voided (~15 vol.%) and the ferrite was relatively void-free; whilst no austenite phases were detected in plate steel. Thermodynamic and phase equilibria software MTDATA has been employed for the first time to investigate neutron irradiation-induced phase transformations. The neutron irradiation effect is introduced by adding additional Gibbs free energy into the system. This additional energy is produced by high energy neutron irradiation and can be estimated from the increased dislocation loop density caused by irradiation. Modelling results show that neutron irradiation reduces the ferrite/austenite transformation temperature, especially for high Ni weld metal. The calculated results exhibit good agreement with experimental observation.

1. Introduction

There is a continuing interest in the use of 9–12%Cr martensitic stainless steels for advanced nuclear applications such as fast reactor core components and first wall structures in proposed fusion devices. The principal benefit associated with these alloys is their excellent resistance to radiation-induced void swelling (e.g. see Little [1] for a detailed data compilation) which is now confirmed to displacement doses exceeding 200 dpa in reactor irradiations of certain grades [2].

Irradiation of these steels induces significant change in microstructure and microchemistry [3], including the production of dislocation loop and network substructures [4], non-equilibrium segregation of solutes to interfaces [5] and precipitate evolution, resulting in both modification of existing phases and the formation of new phases [6,7]. Furthermore, potentially deleterious changes in mechanical properties, such as embrittlement and radiation hardening, are closely related to these microstructural processes. There is therefore considerable motivation in obtaining an in-depth understanding of the development of the irradiation-induced microstructure in order to optimize the irradiation response and hence extend component life time.

The present studies give a detailed analysis of a bulk irradiation-induced phase transformation in a 12%Cr ferritic–martensitic steel weld deposit, involving re-formation (reversion) of austenite from the martensite. The paper also develops a model for the transformation which can explain the principal characteristics in terms of the radiation-induced dislocation loop substructure. Thermodynamic and phase equilibria software MTDATA has been employed for the first time to investigate neutron irradiation-induced phase transformations by introducing additional Gibbs free energy due to neutron irradiation into the system. The weld metal investigated is an off-normal composition prototype containing an enhanced nickel content, designed to explore the limits of irradiation behaviour in the 12%Cr ferritic/martensitic alloy system.

2. Experimental

Parent plate and weld metal of FV448 ferritic/martensitic stainless steel were investigated in this study. The parent plate was supplied in the form of 3 mm thick plate, which was normalized at 1100 °C for 1 h followed by air cool and was tempered at 750 °C for 6 h. Weld metal was produced from plates of FV448 in the half tempered condition (1100 °C/1 h + air cooling + 750 °C/3 h). These plates were welded together via a single pass metal-inert gas process. The weld pool was made off-normal in composition by introducing a small quantity of nickel-rich filler wire. This was

* Corresponding author. Tel.: +44 1509 223168; fax: +44 1509 223949.
E-mail address: zheng.lu@lboro.ac.uk (Z. Lu).

0022-3115/$ - see front matter © 2008 Elsevier B.V. All rights reserved.
doi:10.1016/j.jnucmat.2008.08.007

Table 1
Chemical composition of FV448 plate and weld metal (wt%)

ID	C	Cr	Ni	Si	Mn	Mo	V	Nb
Plate	0.10	10.7	0.64	0.38	1.01	0.64	0.16	0.3
Weld	n/a	13.3	4.7	0.5	0.8	0.8	0.1	0.3

designed to produce a weld composition with enhanced Ni content to 4–5%, but fully martensitic in structure with no-ferrite. Its composition was determined by EDX analysis and shown in Table 1. The weld metal was subsequently given a post weld treatment, corresponding to a full temper, of 6 h at 750 °C. A detailed description of the starting materials, weld fabrication techniques and irradiation procedures, together with preliminary microstructural evaluations are given in a previous publication [8].

FV448 plates and weld metals were irradiated in the core of the Prototype Fast Reactor (PFR) located at Dounreay, UK at an average temperature of 465 °C and to a displacement dose of 28 dpa (NRT), equivalent to an irradiation time of 4656 h. Irradiation procedures and dose and temperature monitoring techniques have been specified previously [9].

In order to separate irradiation phenomena from those due purely to thermal processes, thermal control samples were aged in vacuum at 465 °C for a period of 4656 h.

Thin foils suitable for transmission electron microscopy (TEM) were prepared from the weld metal in the as-tempered, aged and irradiated conditions using discs initially 1 mm in diameter by 0.25 mm thick; these were reconstituted to 3 mm standard diameter with inactive non-magnetic material prior to electropolishing, as described elsewhere [5,10,11]. The reduced volume of active material at this small diameter was originally designed to limit γ-ray emission, but in the present studies has the added advantage of reducing specimen ferromagnetism, thereby enhancing resolution in the TEM.

Microstructural examination of the thin foils was carried out using a Philips EM430T TEM operating at 300 kV, and detailed crystallography of phase transformations evaluated by selected area diffraction (SAD) pattern analysis. It is noted that earlier studies [8] on these weldments emphasized solute segregation effects, which were quantified at interfaces using a Vacuum Generators HB501 field emission scanning electron microscope (FEGSTEM) to provide high resolution solute concentration profiles [12]. These earlier data are referred to in the present paper.

3. Thermodynamic model

Thermodynamic phase equilibria in multicomponent system can be calculated by minimization of the total Gibbs energy G, of all the phases that take part in this equilibrium:

$$G = \sum n_i G^i, \tag{1}$$

where n_i is the number of moles, and G^i is the Gibbs energy of phase i, given by [25]

$$G^i = G^i_T(T,C) + G^i_P(P,T,C) + G^i_M(T_C,\beta_o,T,C), \tag{2}$$

where $G^i_T(T,C)$ is the contribution to the Gibbs energy of phase i by the temperature (T) and the composition (C), $G^i_P(P,T,C)$ is the contribution of the pressure (P) and $G^i_M(T_C,T,\beta_o,C)$ is the magnetic contribution of the Curie or Néel temperature (T_C) and the average magnetic moment per atom (β_0).

When a system is irradiated by high energy particles, such as ions or neutrons, the additional energy due to irradiation is added into the system. The new Gibbs energy of phase i can be expressed by

$$G^i = G^i_T(T,C) + G^i_P(P,T,C) + G^i_M(T_C,\beta_o,T,C) + G^i_{\mathrm{irr}}, \tag{3}$$

where G_{irr} is the contribution to the Gibbs energy of phase i by the neutron irradiation.

The thermodynamic software package MTDATA [20] is employed in this study to predict the relative stabilities of different phases in commercial alloys. The pressure and magnetic contributions are neglected.

The temperature dependence of the concentration term of $G^i_T(T,C)$ is usually expressed in MTDATA as a power series of T [21]

$$G^i_T = a + b\cdot T + c\cdot T\ln(T) + \sum d\cdot T^n, \tag{4}$$

where a, b, c, and d are coefficients, and n is an integer.

Neutron irradiation produces high energy recoils with a wide range of energies. Different nuclear reactors, and corresponding neutron energies, produce different recoil energy spectra. When considering the energy input to the material from the bombarding neutrons, it is not helpful to integrate the area under the neutron energy spectrum [23]. Much of this incoming energy is expended in creating point defects which are quickly annihilated, and much of the bombardment loses its energy in the form of heat. A more useful measure of the energy capture in the real materials is gained from an assessment of the increased permanent defect damage that is created in the irradiated condition. This permanent damage is reflected in the dislocation loop density (It is noted that dislocation loops are thought to be the dominated radiation damage in ferritic/martensitic steels so small vacancy clusters or voids are neglected in this study). The dislocation loop density increases as a function the increased neutron energy and the neutron dose (dpa). Good data on the relation between neutron energy and dose and resultant increased dislocation loop density are available for ferritic pressure vessel steels.

The relation between energy capture and dislocation loop density is given by an assessment of the energy associated with a single dislocation loop (Hirth and Lothe, 1982 Eq. (5)) in the material of interest multiplied by the increased density of dislocation loops caused by the specific irradiation conditions being considered.

$$G^i_{\mathrm{irr}} = 2\pi R\frac{\mu b^2}{4\pi(1-\nu)}\left(\ln\frac{4R}{r_0} - 1\right)\times d_{\mathrm{loop}}, \tag{5}$$

where R is the radius of the circular dislocation loop, μ is the shear modulus of the bulk material, b is the magnitude of the dislocation Burgers vector, ν is the Poisson ratio, r_0 is a dislocation core cut-off radius and d_{loop} is the dislocation loop density.

This energy is fed to the MTDATA thermodynamic package and is regarded as an additional energy to that already possessed by the material in equilibrium at the temperature of interest. The adjustment is made in MTDATA using the access routine.

4. Results and discussion

4.1. Irradiation-induced phase transformation

The microstructure of the modified FV 448 weld metal is fully martensitic in the as-tempered condition, as illustrated in Fig. 1(a), and consists of lath martensite packets within a prior austenite grain boundary network, with the latter aligned in the direction of heat flow.

Thermal ageing at 465 °C produces little change in the microstructure; some reduction in dislocation density and coarsening of precipitates is noted, in agreement with earlier thermal ageing studies at 460 °C to 8250 h on FV448 plate and other l2%Cr steels [2].

The most striking effect of irradiation of the weld metal is the observation of a partial transformation of the initially fully martensitic structure into austenite, resulting in a duplex two-phase microstructure, as illustrated in Fig. 1(b).

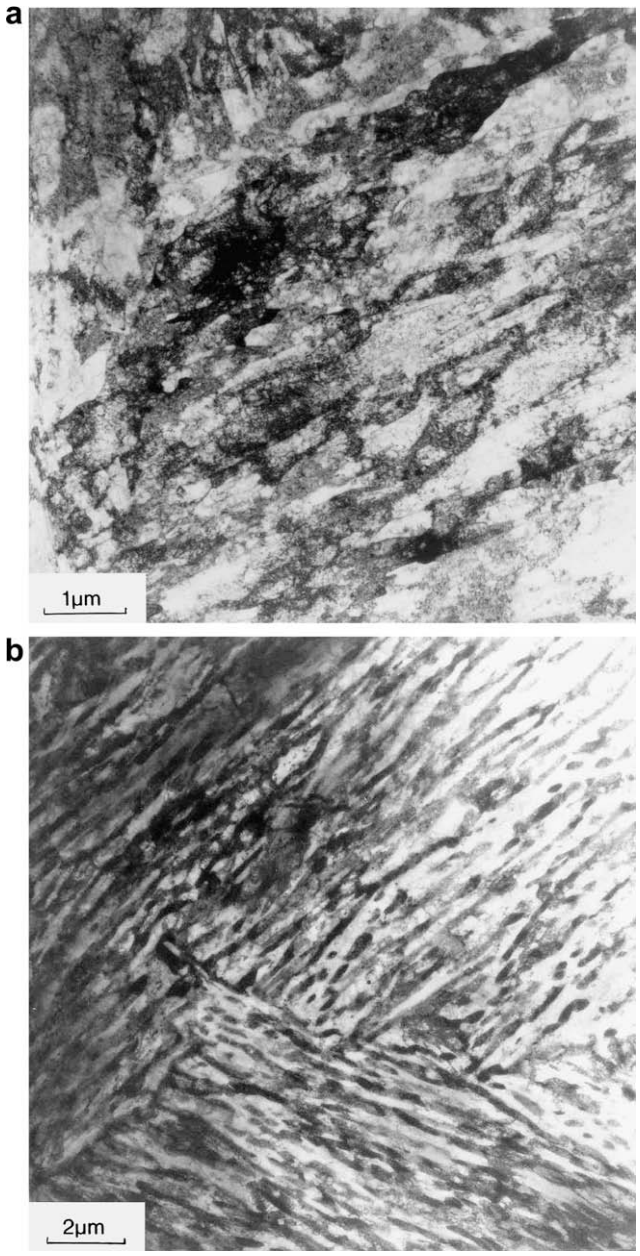

Fig. 1. Transmission electron micrographs of typical microstructures. (a) Unirradiated and (b) irradiated, illustrating lath shaped austenitic phase darkened by diffraction contrast.

This bulk phase transformation was noted in preliminary scoping investigations [8], insofar as islands enriched in nickel and exhibiting localized high levels of void swelling were detected, and thus conjectured to be austenite from these characteristics.

In this study, unequivocable confirmation that the regions are fcc austenitic iron is obtained by indexing diffraction patterns in combination with lattice parameter determinations using the convergent beam microdiffraction technique.

Other detailed features of the transformation which are evident are: (a) the austenite regions are elongated lenticular and lath-shaped; (b) the laths are consistently aligned in a single crystallographic direction within a particular region of the ferrite matrix; and (c) the orientation of the austenite phase relative to the ferrite matrix exhibits well known relationships previously established in the literature to describe the standard austenite-to-martensite transformation, as detailed below.

A complete crystallographic analysis carried out systematically on many laths to determine the orientation of the transformed austenite relative to the matrix ferrite demonstrates the existence of only two orientation relationships. These are both well documented, the first being the Kurdjumov–Sachs (K–S) relationship [13] given by:

$$\begin{aligned} &\{1\,1\,1\}_{fcc}//\{0\,1\,1\}_{bcc},\\ &\langle 0\,1\,1\rangle_{fcc}//\langle 1\,1\,1\rangle_{bcc} \end{aligned}$$

and the second the Nishiyama–Wasserman (N–W) relationship [14–16] defined by:

$$\begin{aligned} &\{1\,1\,1\}_{fcc}//\{0\,1\,1\}_{bcc},\\ &\langle 1\,1\,2\rangle_{fcc}//\langle 0\,1\,1\rangle_{bcc}. \end{aligned}$$

Examples of typical diffraction patterns conforming to the K–S and N–W orientation relations are given in Fig. 2(a) and (b) respectively; in each case the diffraction spots are indexed beside each pattern and the coincidence of spots (viz. reciprocal lattice directions) and zone axes (viz. planes) are given which define the orientation relationship.

In these two examples the agreement is exact; however, in a few cases zone axes with deviations up to 1° from the K–S and N–W relations, as deduced from stereographic projection analysis, are noted, which is within the probable error for the determination by this method.

These single parallel zone axis relationships between the lath austenite and matrix ferrite are generally observed to hold over relatively large areas containing several laths and distances of several microns. In some cases two parallel zone axis relationships – both variants of K–S and N–W – are found to hold within a region of approximately 2 μm diameter as defined by the selected area aperture in the TEM. The significant aspect in these examples is that the transformation product – austenite – exhibits a common crystallographic orientation between the two relationships, and it is the matrix ferrite which is present in two distinct orientations.

4.2. Martensite–austenite reversion mechanism

The present studies demonstrate that a compositionally modified 12%Cr steel weld metal containing a 4.6% Ni addition and with initially fully martensitic structure undergoes partial transformation to austenite following high dose (28 dpa) elevated temperature (465 °C) neutron irradiation.

A comprehensive explanation for this radiation-induced or assisted phase transformation needs to account not only for gross austenite formation, but also for its characteristic lath-like morphology, together with factors leading to transformation via a diffusionless/shear (i.e. martensitic) mechanism. These three aspects are addressed in turn in the following discussion.

4.2.1. Solute segregation

An important link between irradiation and the observed austenite reversion is the changes in composition that occur on a microscopic scale due to radiation-induced non-equilibrium solute segregation (RIS). This process results in coupled transport of solute atoms either towards, or away from, suitable sinks (e.g. interfaces) by point defect fluxes, as a consequence of solute-point defect interactions [17,18]. The mechanism of RIS in ferritic steel have been summarized by Faulkner and coworkers [24,25] and data trends for a broad range of solutes reviewed by Little [3]. It is clear that nickel (the key austenite-forming element) is always enriched at sinks and manganese (another austenite-stabilizer) also exhibits positive segregation in most uses. In contrast, chromium (a ferrite-stabilizer) generally depletes from sinks.

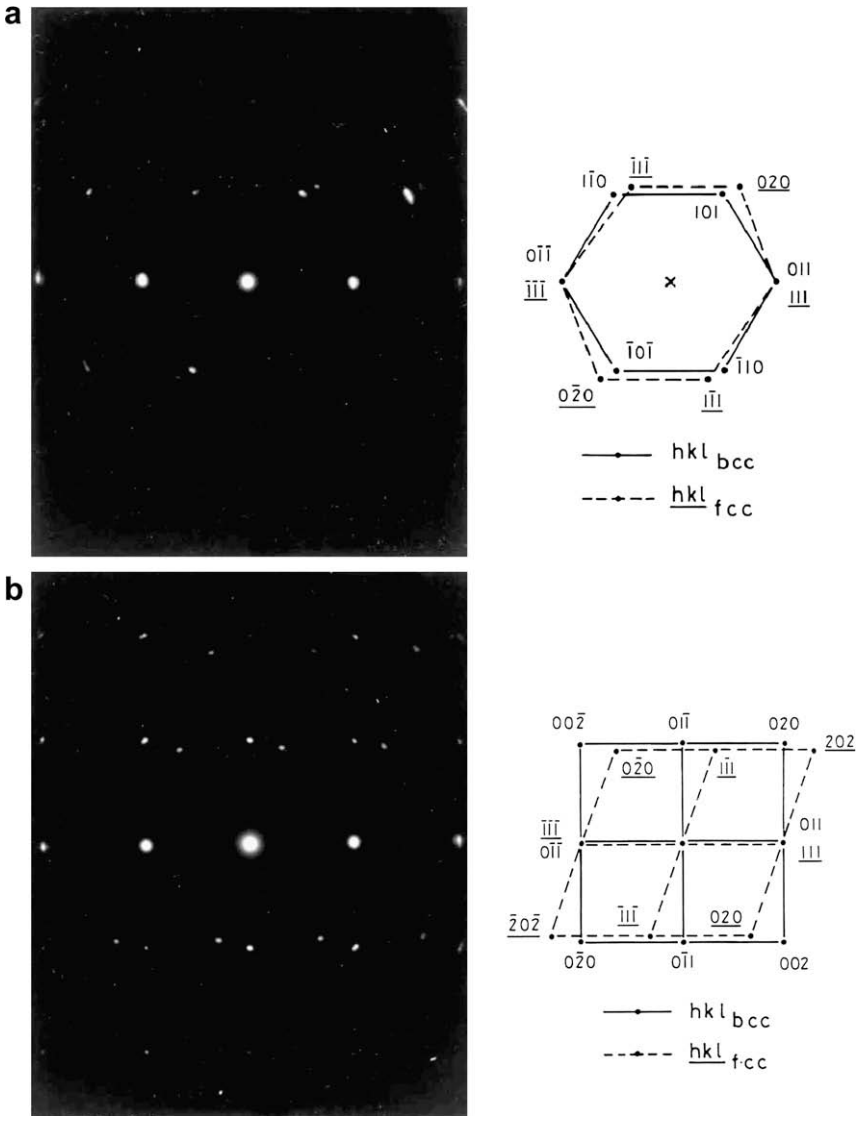

Fig. 2. Selected area diffraction pattern exhibiting indexed and defined coincident zone axis relationships between austenite and ferrite. (a) Kurdjumov–Sachs and (b) Nishiyama–Wasserman.

Hitherto, the only irradiation-induced phase transformations that have been generally reported in ferritic steels are precipitation processes and occur when local solubility limits are exceeded due to solute build-up by RIS; the precipitates are invariably enriched in nickel and other non-typical elements [6]. However, in these steels, only a $\langle 100 \rangle$ loops are generally observed, and this observation provides the basis for a theory for the swelling resistance of ferritic steels [19].

4.2.2. Crystallography

An important feature of the crystallographic relationships found experimentally between the ferrite matrix and the transformed austenite laths – viz. the K–S and N–W orientation relations – is that they have in common that $\{110\}_{bcc}$ planes are parallel to $\{111\}_{fcc}$ planes. A plan view of the stacking-sequence of two adjacent $\{110\}$ layers in a bcc lattice is shown in Fig. 3, with equilibrium stacking positions on lower and upper layers marked a and b, respectively. Also marked are two quasi-equilibrium stacking positions, b′ and b″, lying symmetrically about b, which lie directly above the triangular interstices of the layer below. Translation from b to b′ (or b″) is achieved by a shear of a/8 $[110]$ on a $(10\bar{1})$ plane and is accompanied by a contraction perpendicular to the fault plane.

The operation of such a shear results in the formation of a thin layer of crystal which is close to fcc structure. To illustrate this point, the faulted stacking-sequence of atoms on the $\{110\}_{bcc}$ plane after an a/8 $[110]$ shear are shown in Fig. 4(a); these are compared with the normal stacking-sequence on consecutive $\{111\}$ planes in the fcc crystal, Fig. 4(b). It. is seen that the atom positions are closely similar, and minor relaxations without diffusion can result in coincidence.

4.2.3. Irradiation

The role of irradiation in the formation of this stacking fault arrangement in the bcc structure is now clear. Elevated temperature irradiation creates small a/2$\langle 110 \rangle$ faulted loop nuclei which will unfault at small sizes to an a$\langle 100 \rangle$ perfect geometry via shear of the type a/2 $[110]$. During this shear, the atoms pass directly over the quasi-equilibrium positions b′ and b″. The unfaulting shear thus momentarily causes the atom positions of adjacent $\{110\}_{bcc}$ planes to approximate to those of adjacent $\{111\}_{fcc}$ planes in the ferritic steel regions containing high levels of segre-

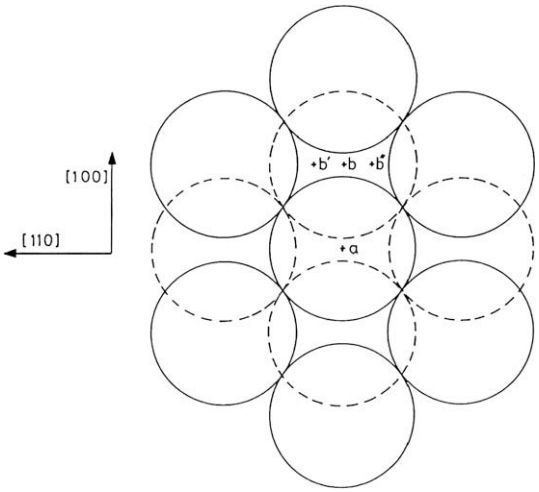

Fig. 3. Plan view of stacking arrangement of adjacent bcc{110} planes, showing both normal and quasi-equilibrium stacking positions.

gated nickel and for which there exists a driving force for transformation to stable austenite. In effect, during unfaulting of a/2⟨110⟩ loop nuclei, the activation energy for this bcc to fcc transformation within the loop is far lower than for transformation from unfaulted bcc crystal. The result is a bcc to fcc austenite shear transformation.

The key supporting evidence for the model lies in the observation of arrays of a⟨100⟩ dislocation loops and loop segments aligned in ⟨100⟩ directions in the irradiated weldment parent plate and in the ferritic regions of the weld which do not transform to austenite [8]. This loop geometry has also been reported previously, and analysed in detail, in FV 448 martensitic steel irradiated to lower doses [4]. It should be made clear that the model proposed in Figs. 3 and 4 represents the results of effecting an a/8⟨110⟩ shear in the {110} plane of the bct structure. The same shear can apply in other planes and for loops in geometries other than a⟨100⟩. Indeed, recent MD and TEM work [26,27] suggest that loops are created with a/2⟨111⟩$_{bct}$ character. Our model can equally well be applied to this case.

4.3. Thermodynamic simulation of martensite-austenite reversion

The extra Ni is anticipated only to lower the A_{c1} from 800 °C for the 10% Cr–0.64% Ni (FV448 composition) parent plate to 720 °C for the weld metal.

In this work, we show that the ferrite-austenite transition temperature is reduced to just below 465 °C (738 K) when a high neutron dose is given to steels of similar composition to the weld

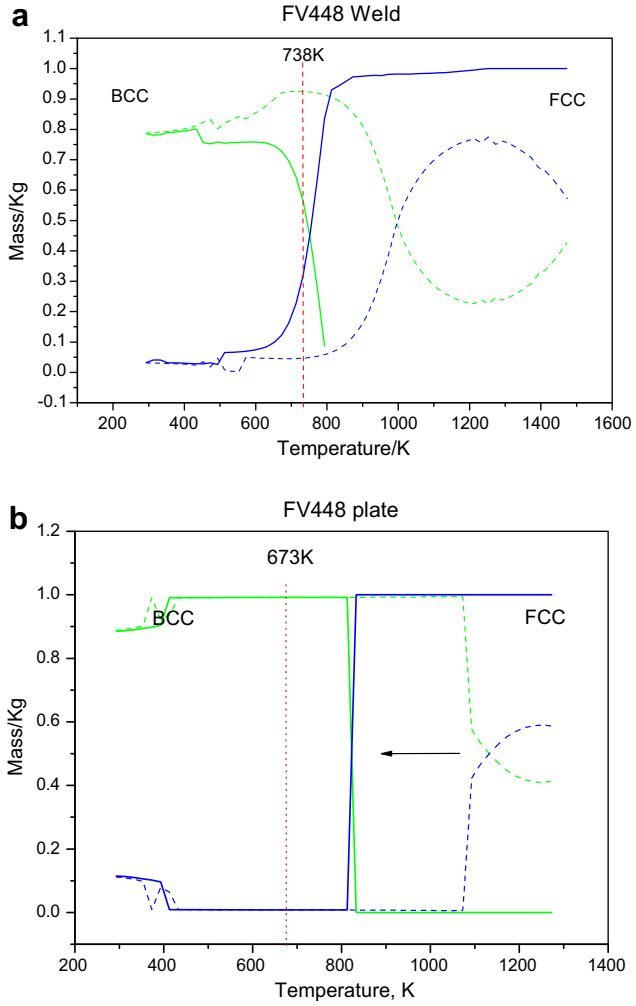

Fig. 5. MTDATA Calculations, show the effect of neutron irradiation on the austenite to ferrite transition temperature in (a) FV448 Weld metal, and (b) FV448 plate. Note: the irradiated (unirradiated) cases are marked by solid (dashed) curves.

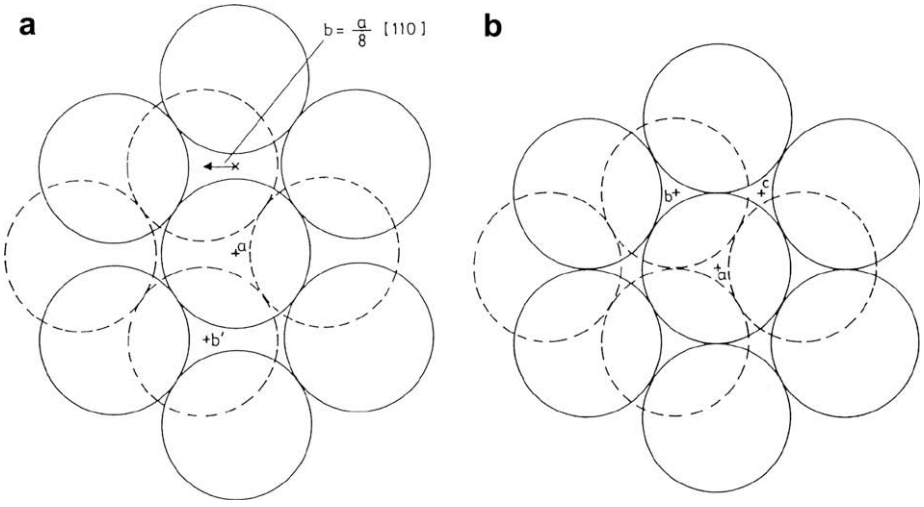

Fig. 4. Comparison between plan views of the stacking arrangements of (a) bcc {110} planes faults by a/8[110] and (b) fcc {111}, normal stacking.

Table 2
Parameters used in this study

Shear modulus of the bulk material μ, GPa	83
Dislocation Burgers vector b, nm	0.248
Poisson ratio v	0.29
Dislocation core cut-off radius r_0, nm	0.72

metal composition (Fig. 5). The underlying data used to forecast such a drop of alpha–gamma transition temperature assumes that the increased dislocation loop density is $3 \times 10^{21}/m^3$, with sizes of 35 nm. This data is obtained from Ref. [22]. Using Eq. (5) this neutron dose is translated into an energy increase of 1030 J mol^{-1}, given to the material. The parameters used are listed in Table 2. This increase is fed to the MTDATA software using Eq. (3).

This result inspires confidence in the approach to the modelling proposed, in that the increased dislocation loop density argument can be applied with reasonable accuracy to forecast the additional energy fed to the material by neutron irradiation to a pre-defined dose.

5. Conclusions

1. A bulk phase transformation to austenite has been investigated in a compositionally modified 12%Cr martensitic steel weld metal containing 4.7 wt% Ni following fast reactor irradiation to 28 dpa at 465 °C.
2. It is suggested that the initial driving force for the transformation is the radiation-induced segregation of austenite-forming elements such as nickel to martensite lath boundaries in the initial microstructure. However, other phenomena are needed to explain the detailed observations.
3. The austenite transformation product exhibits a lath-like lenticular morphology with a specific crystallographic relation to the ferrite matrix which is consistent with formation by a diffusionless/shear mechanism.
4. A model is proposed based on the formation and unfaulting of $a/2\langle 1\,1\,0\rangle$ dislocation loop nuclei under irradiation which provides a low energy path for shear of ferrite to austenite.
5. Thermodynamic and phase equilibria software MTDATA has been employed for the first time to investigate neutron irradiation-induced phase transformations. The neutron irradiation effect is introduced by adding additional Gibbs free energy into the system. This additional energy is produced by high energy neutron irradiation and can be estimated from the increased dislocation loop density caused by irradiation. Modelling results show that neutron irradiation makes the ferrite/austenite transformation occur at a reduced temperature close to the irradiation temperature used in this work, especially for high Ni weld metal.

Acknowledgement

This study is sponsored by EPSRC (Grant No: EP/C510828), UK.

References

[1] E.A. Little, in: D. Kramer, H.R. Brager, J.S. Perrin (Eds.), Proceedings, International Conference on Materials for Nuclear Reactor Core Applications, vol. 2, BNES, London, 1988, p. 41.
[2] D.S. Gelles, J. Nucl. Mater. 212–215 (1994) 114.
[3] E.A. Little, J. Nucl. Mater. 206 (1993) 324.
[4] R. Bullough, M.H. Wood, E.A. Little, in: D. Kramer, H.R. Brager, J.S. Perrin (Eds.), Effects of Radiation on Materials: 10th Conference, ASTM STP, vol. 125, American Society for Testing and Materials, Philadelphia, 1981, p. 593.
[5] T.S. Morgan, E.A. Little, R.G. Faulkner, J.M. Titchmarsh, in: R.E. Stoller, A.S. Kumar, D.S. Gelles (Eds.), Effects of Radiation on Materials: 15th International Symposium, ASTM STP, vol. 1125, American Society for Testing and Materials, Philadelphia, 1992, p. 633.
[6] E.A. Little, L.P. Stoter, ASTM STP 782 (1982) 207.
[7] D.S. Gelles, J. Nucl. Mater. 148 (1987) 136.
[8] T.S. Morgan, E.A. Little, R.G. Faulkner, ASTM STP 1175 (1993) 607.
[9] E.A. Little, D. Stow, J. Nucl. Mater. 87 (1979) 25.
[10] S. Dumbill, W.C. Fuller, Harwell Report AERE-M3640, 1987.
[11] P.K. Rose, J. Rowe, J. Mater. Sci. 22 (1987) 3771.
[12] R.G. Faulkner, T.S. Morgan, E.A. Little, X-ray Spectrometry 23 (1994) 195.
[13] G. Kurdjumov, G. Sachs, Z. Phys. 64 (1930) 325.
[14] Z. Nishiyama, Sci. Rep. Tohoku University, vol. 23, 1934, p. 637.
[15] G. Wasserman, Mit. Kaiser-Wilhelm Institut Eisenforsch. 17 (1935) 149.
[16] G. Wasserman, Arch Eisenhutt. Wes. 16 (1933) 647.
[17] L.E. Rehn, P.R. Okamoto, in: F.V. Nolfi (Ed.), Phase Transformation during Irradiation, Applied Science Publishers Ltd., London, 1983, p. 1.
[18] C.A. English, S.M. Murphy, J.M. Perks, J. Chem. Soc., Faraday Trans. 86 (1990) 1263.
[19] U.R. Kattner, JOM 49 (1997) 14–19.
[20] R.H. Davies, A.T. Dinsdale, T.G. Chart, T.I. Barry, M.H. Rand, High Temp. Sci. 26 (1990) 251.
[21] A.T. Dinsdale, CALPHAD 15 (1991) 317.
[22] E.A. Little, R. Bullough, M.H. Wood, Proc. Royal Soc. London 372 (1980) 565.
[23] R.G. Faulkner, D.J. Bacon, S. Song, P.E.J. Flewitt, J. Nucl. Mater. 271&272 (1999) 1–6.
[24] R.G. Faulkner, R.B. Jones, Z. Lu, P.E.J. Flewitt, Philos. Mag. 85 (2005) 2065.
[25] R.G. Faulkner, S. Song, P.E.J. Flewitt, M. Victoria, P. Marmy, J. Nucl. Mater. 255 (1998) 189.
[26] J. Marian, B.D. Wirth, J.M. Perlado, Phys. Rev. Lett. 88 (2002) 255507.
[27] K. Arakawa, M. Hatanaka, F. Kuramoto, H. Mori, Phys. Rev. Lett. 96 (2006) 125506.